



Research articles

Ferrofluidic Couette flow in time-varying magnetic field

Sebastian Altmeyer

Castelldefels School of Telecom and Aerospace Engineering, Universitat Politècnica de Catalunya, 08034 Barcelona, Spain



ARTICLE INFO

Keywords:

Taylor–couette flow
Ferrofluid
Axial magnetic fields
Alternating magnetic field
Symmetry breaking
Instability
Bifurcations

ABSTRACT

Despite time-dependent boundary conditions being ubiquitous in natural and industrial flows, to date the influence of such temporal modulations (e.g. with driving frequency Ω_H) has been given minor attention. The present problem addresses ferrofluidic Couette flow in between counter-rotating cylinders in a spatially homogeneous magnetic field subject to time-periodic modulation. Such a modulation can lead to a significant inner Reynolds number (Re_i) enhancement for both, either helical and toroidal flow structures. Using a modified Niklas approximation, the effect of low- and high-frequency modulation onto the primary instabilities, stability boundaries as well as on the non-linear oscillations that may occur is investigated. Focusing on bi-stable co-existing solutions, around their stability thresholds quite complex non-linear system response and flow dynamics is detected. For the system remaining supercritical always a *single solution* is selected by Ω_H , while crossing the bifurcation thresholds within a modulation period the triggered system response is more complex, reaching from alternation between different solutions towards the appearance of intermittent behavior.

1. Introduction

The system setup of two concentric cylinders with different radii which can rotate independently of each other – Taylor–Couette system (TCS) [1,2] – and external temporally forcing presents paradigm problem for the parametric control of flow instability and pattern formation. Consider classical TCS with Newtonian fluid such forcing has been typically imparted mechanically into the system. Most common types are harmonically modulated rotations of either the inner or outer cylinder (or both), harmonic oscillations of one cylinder in the axial direction, pulsation of an axial imposed flow or even radial through flow [3–12]. However, all these works have one thing in common; the new effects and resulting flow modifications are introduced by modified *boundary conditions*.

Instead, consider a magnetic fluid, e.g. a ferrofluid [13,14], offers the unique advantage to maintain a *stationary* setup while introducing any periodic forcing direct into the fluid within the bulk exposed to external magnetic fields. Thereby ferrofluids, are a suspension of permanently magnetized colloidal particles, which present a scientifically and commercially important realization of magnetic fluids [13,14]. Mechanical, magnetic, and chemical properties make ferrofluids of interest in the design of microfluidic pumps driven by alternating or rotating magnetic fields. Within ferrofluids the magnetization \mathbf{M} is often *not* collinear with the applied magnetic field \mathbf{H} resulting from coupling of viscous and magnetic torques with rotational Brownian motion, which can result in significant changes in flow structures and dynamics. So far various numerical and experimental studies of ferrofluidic Couette

flows consider static magnetic fields focusing on different field orientations, agglomeration, internal magnetization and other effects [15–26]. Common conclusion of all these works is the fact that a stationary magnetic field, independent its orientation *stabilizes* the basic state (Circular Couette flow, CCF), i.e. the bifurcation threshold of the primary instabilities are shifted to larger values of the control parameter (most common the inner Reynolds number Re_i). Special focus has also been given to the magneto-viscous effect, i.e. the increase in viscosity of a ferrofluid in presence of a magnetic field [13,27,28]. Physical explanation is that a present magnetic field causes a partial orientation of magnetic moments of the particles, and thereby preventing their free rotation in the flow. However, in an alternating magnetic field the additional viscosity is *negative* at high driving frequencies and positive at low driving frequencies [29]. This is a consequence of an induces rotatory oscillations of the particles by the alternating field, without any favored direction of rotation, i.e. zero in average. The final non-zero angular velocity of the particles is caused by the presence of shear, which breaks down the degeneracy of the direction of rotation.

The recent review by Kole and Khandeka [30] provides a detailed overview of engineering applications of ferrofluids, reaching from design applications in machine elements over Bio-medical applications to the use in thermal engineering. Aside the general interest in engineering the understanding of fundamental physical and chemical aspects ferrofluids offer great opportunities for *medical applications* and future developments. One target is the exact and close positioning of a drug near an organ needing treatment and therefore to reduce unwanted

E-mail address: sebastian.andreas.altmeyer@upc.edu.

<https://doi.org/10.1016/j.jmmm.2022.169205>

Received 16 July 2021; Received in revised form 9 January 2022; Accepted 18 February 2022

Available online 26 February 2022

0304-8853/© 2022 Elsevier B.V. All rights reserved.

side effects. Here the surfactant molecules of a ferrofluid offer the opportunity to attach such drugs, which then, after injection of the drug-carrying fluid into a blood vessel can be concentrated at a desired position by applying a strong magnetic field gradient [31]. By doing so, the drug can be localized in the body at position where treatment is required and thus minimizing any undesired effects on health tissue around. Further opportunities lie in the therapy technique for cancer treatment by hyperthermia. Enriching fluid particles that are marked with tracer substances in the tumor tissue, an alternating magnetic field can be applied while the energy losses due to magnetization change in the particles can be used to heat up the tissue [32]. This allows avoiding side effects to other organs while destroying the tumor.

Over the years, molecularly targeted therapies have significantly advanced, but the delivery across the blood–brain barrier and the targeting of brain tumors remains a difficult challenge. The recent work by Wu et al. [33] presents a big step forward in this challenging task. They fabricated a new aqueous, surfactant-free ferrofluid with superparamagnetic iron oxide nanoparticles which is coated with silicate mesolayers and carbon shells and illustrated that such a ferrofluid has special physiochemical and biological properties, e.g. colloidal stability and can significantly improve cancer targeting procedures.

More recently alternatives to the common and well established magnetite (APG series [34]) and Cobalt based ferrofluids have been manufactured and studied. One of such examples is the hybrid nanofluid composed of kerosene and ZnO-Al₂O₃ nanoparticles studied by Zhang et al. [35]. Investigating flow and heat transfer of this hybrid nanofluid variations in velocity and temperature profiles are found by increasing the magnetic field parameter.

To date, investigations of ferrofluid under alternating magnetic fields are relatively rare and aside the former mentioned viscosity studies [29] they are given mostly special attention to heat behavior [36,37]. Most prominent observation for ferrofluidic flows under alternating fields is the fact that sufficiently high modulation frequency will force a faster rotation of the particles [29]. More recently for outer cylinder at rest it has been shown that a time-periodic modulated magnetic field also stabilizes the basic state with respect to axisymmetric Taylor vortex flow (TVF) [38]. Furthermore, such an alternating magnetic field can provide an accurate control parameter to balance the system to be either sub- or supercritical. Similar studies for flow control of ferrofluids due to external applied magnetic fields have been carried out in various systems. For laminar flow between parallel plate channels [39] the external applied field is found to uniquely modify the local velocity distribution and to reduce the effect of both adverse and favorable pressure gradients and thus allow to control the flow separation. Also an early, but prospective application of ferrofluids is in damping [40]. Most common of such ferrofluid damping devices are dampers, vibration isolators, and dynamic vibration absorbers whereby their simplicity, flexibility and reliability gives them a prominent advantage compared with conventional damping devices.

The aim of this paper is to numerically investigate effects induced on ferrofluidic Couette flow by an externally applied time-periodic magnetic field. Counter-rotating cylinders are used to investigate either toroidal closed (TVF) and helical (SPI) flow structures and to guarantee bistability between different solutions close to their onsets. We observe significant enhancement in system stability against the different primary instabilities. Special focus is given to the non-linear system response for bistable existing TVF and SPI and their behavior for sub- and supercritical parameters with respect to the driving frequency. Depending on the latter the system features characteristics of intermittency. These findings may, among others contribute to applications of ferrofluids in damping systems, where different alternating frequency will allow for accurate system response in the sense of controllable and specific desired damping characteristics.

Table 1

Parameters and their ranges investigated in this paper.

Parameter	Symbol	Range
Inner Reynolds number	Re_i	[110; 190]
Outer Reynolds number	Re_o	-125
Axial wavenumber	k	3.927
Static contribution	$s_{z,S}$	[0; 1.0]
Modulation amplitude	$s_{z,M}$	[0; 1.0]
Modulation frequency	Ω_H	$[10^{-3}; 10^4]$

2. Methods

2.1. System parameters

Flow strength in TCS (Fig. 1(a)) is commonly represented in terms of the inner [outer] Reynolds number $Re_{i[o]} = \omega_{i[o]} r_{i[o]} d / \nu$, characterizing the ratio between inertia and viscous forces. These have been proven to be very well suited parameters to describe the driving of the system [41]. Here $r_{i[o]}$ is the non-dimensionalized inner [outer] radius and $\omega_{i[o]}$ the angular velocity of the inner [outer] cylinder. Periodic boundary conditions are imposed in axial (z) direction and no-slip boundary conditions on the cylinder surfaces. The cylindrical coordinate system (r, θ, z) by the velocity field $\mathbf{u} = (u, v, w)$ and the corresponding vorticity field $\nabla \times \mathbf{u} = (\xi, \eta, \zeta)$ can be used to characterize the system. In this work the radius ratio of the cylinders is kept fixed at 0.5 and further a counter-rotating system setup is considered with fixed outer Reynolds number $Re_o = -125$. The time, and length scales are made dimensionless by diffusion time d^2/ν and gap width d and the pressure in the fluid is normalized by $\rho\nu^2/d^2$.

To realize a periodically modulated TCS, we apply a sinusoidal modulation signal to the external magnetic field, which is orientated parallel to the system symmetry (z) axis, uniform in space and harmonic in time $\mathbf{H}_z = [H_S + H_M \sin(\Omega_H t)]\mathbf{e}_z$. Important to mention that in case of a static magnetic field ($H_m = 0$) such a *pure* axial oriented magnetic field does *not* change the system symmetry. Only stability thresholds are shifted as previously reported [21–23]. The magnetic field \mathbf{H} and the magnetization \mathbf{M} are conveniently normalized by the quantity $\sqrt{\rho/\mu_0}\nu/d$, with free space permeability μ_0 . By using a modified Niklas approach [17,22,38] the effect of the magnetic field and the magnetic properties of the ferrofluid on the velocity field can be characterized by a single (time dependent) parameter

$$s_z(t) = s_{z,S} + s_{z,M} \sin(\Omega_H t), \quad (1)$$

with $s_{z,S}$ being the *static contribution* of the driving, $s_{z,M}$ the *modulation amplitude*, and Ω_H the *modulation frequency*. See Methods Section 2 for more details.

2.2. Explored parameter space

The current paper explores the parameter space within $0 \leq s_{z,S}, s_{z,M} \leq 1$. The trajectories I and II shown in the schematics illustrating the parameter space of Fig. 1(b) represent pure *static* and pure *alternating* magnetic fields, respectively. Point A presents the parameters for both bi-stable and coexisting supercritical flows, wavy Taylor Vortex flow (wTVF) and spiral vortex flow (spiral, SPI) at $Re_i = 141$, respectively (cf. Fig. 3). The trajectories III and IV highlight the parameters at which we provide a more detailed study around the onsets of instability at point A for $Re_i = 141$ (cf. Fig. 2) (see Table 1).

2.3. Ferrohydrodynamical equation of motion

The non-dimensionalized hydrodynamical equations [23,25,43] are derived from:

$$(\partial_t + \mathbf{u} \cdot \nabla)\mathbf{u} - \nabla^2\mathbf{u} + \nabla p =$$

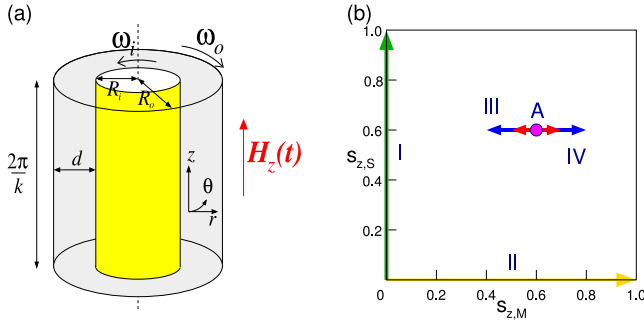


Fig. 1. System and explored parameter space. (a) Schematic of the Taylor-Couette system (TCS) with an external applied homogeneous magnetic field $\mathbf{H}_z(t) = [H_S + H_M \sin(\Omega_H t)]\mathbf{e}_z$. (b) The arrows I and II indicate the investigated parameter space for $0 \leq s_{z,S}, s_{z,M} \leq 1$. Point A gives the parameters for supercritical flows at $Re_i = 141$ while III and IV correspond to the set of parameters around the stability threshold and the onset of instability.

$$\begin{aligned} (\mathbf{M} \cdot \nabla)\mathbf{H} + \frac{1}{2}\nabla \times (\mathbf{M} \times \mathbf{H}), \\ \nabla \cdot \mathbf{u} = 0 \end{aligned} \quad (2)$$

The velocity fields on the cylindrical surfaces are $\mathbf{u}(r_i, \theta, z) = (0, Re, 0)$ and $\mathbf{u}(r_o, \theta, z) = (0, 0, 0)$, with the inner [outer] Reynolds numbers $Re_{i[o]} = \omega_{i[o]} r_{i[o]} d / \nu$, where $r_{i[o]} = R_{i[o]} / (R_o - R_i)$ is the non-dimensionalized inner [outer] cylinder radius.

Eq. (2) is solved with an equation describing the magnetization of the ferrofluid. Here we consider an equilibrium magnetization of an unperturbed state with homogeneously magnetized ferrofluid at rest. Thereby the mean magnetic moment is orientated (aligned) in the direction of the magnetic field: $\mathbf{M}^{\text{eq}} = \chi \mathbf{H}$. Langevin's formula [44] is used to approximate the ferrofluid's magnetic susceptibility χ . Further initial value χ is set to be 0.9 with use of a linear magnetization law. Here we consider the ferrofluid APG933 [34,45]. The near equilibrium approximation by Niklas [17,46] assumes small derivations $\|\mathbf{M} - \mathbf{M}^{\text{eq}}\|$ and small magnetic relaxation time $\tau: |\nabla \times \mathbf{u}| \tau \ll 1$. Using these approximations, one can obtain [25] the following magnetization equation:

$$\mathbf{M} - \mathbf{M}^{\text{eq}} = c_N^2 \left(\frac{1}{2} \nabla \times \mathbf{u} \times \mathbf{H} + \lambda_2 \mathbb{S} \mathbf{H} \right), \quad (3)$$

where

$$c_N^2 = \tau / (1/\chi + \tau \mu_0 H^2 / 6\mu\Phi) \quad (4)$$

is the Niklas coefficient [17], μ is the dynamic viscosity, Φ is the volume fraction of the magnetic material, \mathbb{S} is the symmetric component of the velocity gradient tensor [25,43], and λ_2 is the material-dependent transport coefficient [43], which we choose to be $\lambda_2 = 4/5$ [26,43,47,48]. Using Eq. (3), the magnetization in Eq. (2) can be eliminated to obtain the following ferro-hydrodynamical equations of motion [23,25,38,43]:

$$\begin{aligned} (\partial_t + \mathbf{u} \cdot \nabla)\mathbf{u} - \nabla^2 \mathbf{u} + \nabla p_M \\ = -\frac{s_z}{2} \left[\mathbf{H} \nabla \cdot (\mathbf{F} + \frac{4}{5} \mathbb{S} \mathbf{H}) + \mathbf{H} \times \nabla \times (\mathbf{F} + \frac{4}{5} \mathbb{S} \mathbf{H}) \right], \end{aligned} \quad (5)$$

where $\mathbf{F} = (\nabla \times \mathbf{u})/2 \times \mathbf{H}$, p_M is the dynamic pressure incorporating all magnetic terms that can be expressed as gradients, and s_z is the Niklas function (classical a static parameter) [Eq. (7)]. To the leading order, the internal magnetic field in the ferrofluid can be approximated as the externally imposed field [23], which is reasonable for obtaining dynamical solutions of the magnetically driven fluid motion. Further simplification of Eq. (5) leads to

$$\begin{aligned} (\partial_t + \mathbf{u} \cdot \nabla)\mathbf{u} - \nabla^2 \mathbf{u} + \nabla p_M = s_z^2 \left\{ \nabla^2 \mathbf{u} - \frac{4}{5} [\nabla \cdot (\mathbb{S} \mathbf{H})] \right. \\ \left. - \mathbf{H} \times \left[\frac{1}{2} \nabla \times (\nabla \times \mathbf{u} \times \mathbf{H}) - \mathbf{H} \times (\nabla^2 \mathbf{u}) + \frac{4}{5} \nabla \times (\mathbb{S} \mathbf{H}) \right] \right\}. \end{aligned} \quad (6)$$

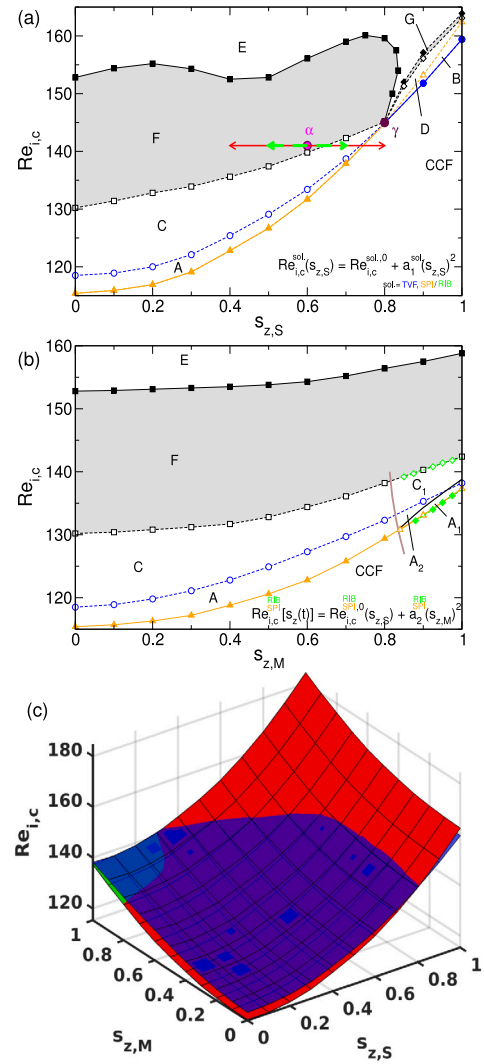


Fig. 2. Stability in magnetic fields. Phase diagram for TVF, SPI, wTVF, wSPI and RIB in (a) a static magnetic field as a function of $s_{z,S}$ and (b) a modulated magnetic field as a function of $s_{z,M}$ (cf. trajectory II in Fig. 1(b)), respectively. The bifurcation thresholds for TVF and SPI/RIB, out of CCF are denoted by the blue line with circles and the orange line with triangles, respectively. Filled (open) symbols indicate that the respective solution is stable (unstable) at threshold. Both TVF and SPI are stable in region E. The black solid lines describe the upper bifurcation thresholds of wTVF (■) and wSPI (◆) out of TVF and SPI, respectively. The wavy structures are stable in the respective gray colored regions G and F (a, b) and become unstable at the black dashed curve with open symbols (□, ◇). Different solutions and their corresponding stability in the various regions are listed in Table 3. Note that regions are indicated with the same labels as already introduced in [42] (cf. Fig. 3). With respect to static magnetic fields (a), the stability thresholds for TVF and SPI/RIB can be approximated by the function $Re_{i,c}^{\text{sol}}(s_{z,S}) = Re_{i,c}^{\text{sol},0} + a_1^{\text{sol}} s_{z,S}^2$ (sol.={TVF,SPI/RIB}), $a_1^{\text{TVF}} = 41.0$, $a_1^{\text{SPI/RIB}} = 46.9$ where $Re_{i,c}^{\text{sol},0}$ is the stability threshold in absence of any magnetic field. A similar approximation can be found for the SPI/RIB stability threshold under modulated magnetic fields (b) via $Re_{i,c}^{\text{SPI/RIB}}(s_z(t)) = Re_{i,c}^{\text{SPI/RIB},0} + a_2^{\text{SPI/RIB}} s_{z,M}^2$ (SPI/RIB $a_2^{\text{SPI/RIB}} = 21.8$). Note, the For TVF the dependence under modulated fields is more complex and cannot be approximated by a simple quadratic formula. (c) Surface illustrating the critical Reynolds number $Re_{i,c}$ over $(s_{z,S}, s_{z,M})$ -plane for TVF (blue) and SPI/RIB (red/green). Note, SPI and RIB exist degenerated. The thick violet point in (a) denotes the 'bi-critical point' γ .

This way, the effect of the magnetic field (here homogeneous but alternating with $\mathbf{H}_z = [H_S + H_M \sin(\Omega_H t)]\mathbf{e}_z$ and the magnetic properties of the ferrofluid on the velocity field can be characterized by a single function, the magnetic field or the (here time dependent) Niklas

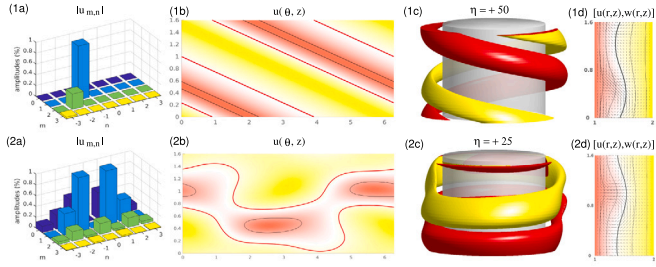


Fig. 3. Supercritical bi-stable existing flow states SPI (1) and wTVF (2) for $Re_i = 141$ (cf. point A in Fig. 1(b) and point α in Fig. 2(a)). Visualization of (1) SPI and (2) wTVF. Shown are (a) mode amplitudes $|u_{m,n}|$ of the Fourier spectrum (m, n) , (b) the radial velocity $u(\theta, z)$ on an unrolled cylindrical surface in the annulus at mid-gap [red (yellow) color indicates in (out) flow], (c) isosurfaces of η [red (dark gray) and yellow (light gray) colors correspond to positive and negative values, respectively, with zero specified as white] and (d) vector plot $[u(r, z), w(r, z)]$ of the radial and axial velocity components (including the azimuthal velocity v . The thick contour lines correspond to $v/Re_i = 0.5$.

function [17]:

$$s_z(t) = \sqrt{c_N} H_z = \sqrt{c_N} [H_S + H_M \sin(\Omega_H t)] \quad (7)$$

$$= s_{z,S} + s_{z,M} \sin(\Omega_H t),$$

with the two *time-independent* “Niklas” control parameters

$$s_{z,S} = \sqrt{c_N} H_S \quad \text{and} \quad s_{z,M} = \sqrt{c_N} H_M \quad (8)$$

standing for the static contribution ($s_{z,S}$) and the modulation amplitude ($s_{z,M}$) of the driving, respectively.

2.4. Numerics

The ferrohydrodynamical equations of motion Eq. (5) are solved [17,22,23,25,49] by a standard, second-order finite-difference scheme in (r, z) combined with a Fourier spectral decomposition in θ and (explicit) time splitting. In the present work we consider periodic boundary conditions in axial direction corresponding to a fixed axial wavenumber $k = 3.927$. On the cylinder surfaces, no-slip boundary conditions are used and the radius ratio of inner and outer cylinders is kept fixed at $r_i/r_o = 0.5$. The variables in the finite-difference scheme in (r, z) can be expressed as

$$f(r, \theta, z, t) = \sum_{m=-m_{\max}}^{m_{\max}} f_m(r, z, t) e^{im\theta}, \quad (9)$$

where f denotes one of the variables $\{u, v, w, p\}$. For the parameter regimes considered, the choice $m_{\max} = 16$ provides adequate accuracy. Explicit time splitting is used. The explored parameter range spans $110 \leq Re_i \leq 190$, $0 \leq s_{z,S}, s_{z,M} \leq 1$, and $10^{-3} \leq \Omega_H \leq 10^4$. For these parameters, the choice of 16 azimuthal modes provides adequate accuracy. Uniform grid with spacing $\delta r = \delta z = 0.02$ and time steps $\delta t < 1/3800$ are used. For diagnostic purposes, we also evaluate the complex mode amplitudes $f_{m,n}(r, t)$ obtained from a Fourier decomposition in the axial direction:

$$f_m(r, z, t) = \sum_n f_{m,n}(r, t) e^{inkz}, \quad (10)$$

where $k = 2\pi d/\lambda$ is the axial wavenumber. The Appendix provides a brief comparison with experimental results and relates the non-dimensional Niklas function with physical values for the applied magnetic field H .

2.5. Brief remarks on symmetries

In absence of any periodic forcing the symmetry group of the Taylor–Couette problem is $O(2) \times SO(2)$ [2]. The basic state is invariant

Table 2

Flow state nomenclature and abbreviations. From left to right; acronym, flow state, dominant azimuthal (mode) contribution and flow dynamics, and topological classification as fixed point (f) or limit cycle (l). Note, SPI exist degenerated as left- ($m = +1$) and rightwinding ($m = -1$) solutions.

Acronym	Flow state	Dominant modes m	Dynamics	Solution
TVF	Taylor-Vortex flow	0	–	f
wTVF	Wavy Taylor-Vortex flow	0 ± 1	Rotating	l
SPI	Spiral vortex flow	+1	Rotating	l
wSPI	Wavy spiral vortex flow	$+1, \pm 2$	Rotating	l
RIB	Ribbon	± 1	Rotating	l

to a number of symmetries whose actions on a general velocity field are

$$R_\Phi(u, v, w)(r, \theta, z) = (u, v, w)(r, \theta + \Phi, z)$$

$$K_z(u, v, w)(r, \theta, z) = (u, v, -w)(r, \theta, -z) \quad (11)$$

$$T_\beta(u, v, w)(r, \theta, z) = (u, v, w)(r, \theta, z + \beta)$$

The $SO(2)$ represents the rotational symmetry in the azimuthal direction. The presence of purely axial imposed magnetic field does not change the symmetry group and $O(2) \times SO(2)$ remains the symmetry group for the periodically forced system. While $SO(2)$ remains unaffected due to the modulation, the axial reflection is no longer a symmetry of the problem. Instead, composing with a half-period time translation one obtains a glide-time symmetry G of the system. This symmetry, together with axial translations, still gives the symmetry group $O(2)$. Explicit acting on the velocity fields, one obtains following expression of this symmetry (half-period-flip-symmetry),

$$G(u, v, w)[r, \theta, z, t] = (u, v, -w)[r, \theta, -z, t + T_H/2]. \quad (12)$$

With this R changes from a purely spatial symmetry to a space-time symmetry. A consequence of the space-time Z_2 symmetry generated by G implies a more complex bifurcation scenario, e.g. inhibiting period doubling via a simple negative eigenvalue $\mu = -1$ [4,50]. Note that T_H is the period time of the applied magnetic field.

2.6. Nomenclature

The present study focus on flow dynamics in TCS with axial wavenumber $k = 3.917$, equivalent to a small aspect-ratio $\Gamma = 1.6 = 2\pi/k$, and counter-rotating cylinders for fixed outer Reynolds number $Re_o = -125$, while the inner Reynolds number varies $110 \leq Re_i \leq 170$ (i.e. rotation ratio equal $-1.14 \lesssim Re_o/Re_i \lesssim -0.74$, respectively). As a result common appearing structures in *absence* of any magnetic field are well known flow states, (w)TVF, (w)SPI and RIB [1,2,41,42,51–53]. Table 2 provides an overview of all different flow states discussed in this work. Acronyms, flow states, including dominant modes, flow dynamics, and topological classification are indicated. As only pure axial magnetic fields are considered the standard system symmetries are preserved [21,22].

3. Results

3.1. Stability behavior

First we will investigate how a modulated magnetic field effects the primary instabilities, i.e. the stability thresholds of SPI/RIB and TVF, respectively. Note, that SPI and ribbon (RIB) appear at a common bifurcation threshold, with RIB being a non-linear superposition of two SPI with opposite helical orientation. Strictly speaking the solution has to be identified as 1-SPI [1-RIB] with azimuthal wavenumber $M = 1$ [$m = \pm 1$]. But as for given parameters only 1-SPI [1-RIB] appear, it is sufficient to use the generic term SPI [RIB] in the following.

Table 3

Various regions, labeled A-G, as presented in the $(Re_{i,c}, s_{z,S})$ and $(Re_{i,c}, s_{z,M})$ parameter space diagrams (Fig. 2(a, b)) including their stability properties (stable (s), unstable (u), non-existent (-)).

Region	A	A ₁	A ₂	B	C	C ₁	D	E	F	G
TVF	-	-	-	s	u	u	s	s	u	s
SPI	s	u	s	-	s	s	u	s	s	u
wTVF	-	-	-	-	-	-	-	-	s	-
wSPI	-	-	-	-	-	-	-	-	-	s
RIB	u	s	u	-	u	s	u	u	u	s

3.1.1. Static magnetic fields: $s_{z,M} = 0$

Concerning static magnetic fields various studies [17,20–23] have shown that any applied magnetic field regardless its orientation *stabilizes* the CCF basic state, i.e. shifting the bifurcation thresholds to larger control parameter (e.g. Re_i). Without magnetic fields, i.e. $s_z = 0$, the critical values are $Re_{i,c}^{SPI,0} = 115.4$ and $Re_{i,c}^{TVF,0} = 118.5$, respectively. Note, that other axial wavenumber (here $k = 3.927$) will lead to other critical Reynolds numbers Re_c^0 . The stabilization with static field strength $s_{z,S}$ can be approximated with a power law according to $Re_{i,c}^{sol.}(s_{z,S}) = Re_{i,c}^{sol.,0} + a_1^{sol.} s_{z,S}^2$ (with sol. standing for the solutions TVF, SPI/RIB, respectively; constants $a_1^{TVF} = 41.0$, $a_1^{SPI/RIB} = 46.9$, respectively) (see Fig. 2(a)). Both, TVF and SPI/RIB are *different strong* affected by increasing $s_{z,S}$, which also result in an exchange in the primary stable bifurcating solution. Thus, the bifurcation threshold cross in the point of higher co-dimension, γ , and exchange stability at $s_{z,S} \approx 0.812$ in Fig. 2(a). (See also [42] for further details.)

The various regions, labeled A-G, as indicated in Fig. 2(a, b) identify the existence and stability [stable (s), unstable (u), non-existent (-)] of the different solutions for here investigated parameter space. As this is not the main topic of the current paper we refer to former works [42,49] for further details regarding the stability and transition between the different solutions. We keep the same notation/labels as already introduced in the work [42] (c.f. Fig. 3).

3.1.2. Modulated magnetic fields: $s_{z,M} \neq 0$

A detailed study regarding stability behavior and bifurcation behavior of TVF, SPI and RIB under the influence of modulated magnetic field can be found in [49]. Here we will only summarize the most important features. Increasing the modulation amplitude $s_{z,M}$ (Fig. 2(b)) stabilizes the CCF basic state while the magnitude depends on the corresponding flow structure SPI/RIB or TVF. Thereby *no* crossing in the bifurcation thresholds and thus no stability exchange appears for here studied parameters. However, for sufficiently strong modulation amplitude $s_{z,M} \approx 0.82$ stability is exchanged between SPI and RIB. For $s_{z,M} \lesssim [\gtrsim] 0.82$ SPI [RIB] appears stable out of the common bifurcation threshold while RIB [SPI] is unstable close to onset [2,42,54]. For SPI/RIB, the stabilization of the CCF basic state can be quantified with an approximate power law according to $Re_{i,c}^{SPI/RIB}(s_z(t)) = Re_{i,c}^{SPI/RIB,0} + a_2^{SPI/RIB} s_{z,M}^2$, with $a_2^{SPI/RIB} = 21.8$ (Fig. 2(c)). This is very similar to the stabilization for static fields. For TVF the dependence under modulated fields is more complex and cannot be approximated by such a simple quadratic formula.

Finally, Fig. 2(c) presents the bifurcation thresholds $Re_{i,c}^{sol.}$, sol. \in (SPI,RIB,TVF) (over $(s_{z,S}, s_{z,M})$ -plane) for TVF (blue) and SPI/RIB (red/green), respectively. Note that this visualization only shows the thresholds and not necessary the stability of the solution. In principle the lower (higher) surface (i.e. smaller $Re_{i,c}$) indicates a stable (unstable) bifurcating solution. The thresholds for SPI and RIB are identical [2,42,54] while RIB are mainly unstable at onset; the green highlighted region illustrate RIB to bifurcate stable, while SPI appear unstable and vice versa for the red surface. Common feature of all surfaces is that they are convex in any direction.

For parameters in Fig. 2 the maximum stability enhancement in $Re_{i,c}^{SPI/RIB/TVF}$ is about 62.6% for SPI/RIB and 66.8% for TVF, comparing the system in absence of any magnetic field with alternating magnetic field at $(s_{z,S} = 1 = s_{z,M})$.

To summarize, in terms of stability the system reacts to an alternating modulation of the magnetic field similar as increasing the magnetic field strength in the static case. This holds for all solutions SPI, RIB and TVF, while the effect, i.e. the magnitude of stabilization is stronger for the helical states SPI/RIB. As a result the primary bifurcation thresholds cross and exchange stability (Fig. 2(c)). The stabilization increase with increasing modulation amplitude can be understood by the static field behavior in particular its non-linear grows with power of 2 (Fig. 2(a)). Therefore, during one modulation period the system experience a stronger stabilization effect while the modulation amplitude is above (positive) the average field strength in comparison to the destabilization in the other half period when it is below (negative) the average field strength. As a result the stabilization within an modulated magnetic field corresponds to a static field strength, which lies *above* the mean value of the alternating field [49]. In analogy, with increasing modulation amplitude (Fig. 2(b)) also the stabilization effect grows.

Worth mentioning that for those parameters $s_{z,M}$ at which RIB appear stable also the whole wTVF branch connecting RIB and TVF becomes stabilized. This was already speculated for the classical system [42] but as wTVF become unstable with approach to RIB a ‘jump’ bifurcation [51] towards SPI appears, and confirmed in the recent work for modulated magnetic fields [49].

3.2. Dynamic system response

In order to investigate the dynamic system response we need well-defined initial states. Consider supercritical SPI and wTVF at $Re_i = 141$ and fixed static field contribution $s_{z,S} = 0.6$ ($s_{z,M} = 0$), equal to $\mu = Re_i(s_z(t))/Re_{i,c}^{SPI,0}(s_{z,S} = 0.6) - 1 = 0.071$ and $\mu = Re_i(s_z(t))/Re_{i,c}^{TVF,0}(s_{z,S} = 0.6) - 1 = 0.057$ (far away from the onsets of the respective instability $Re_{i,c}^{SPI}(s_{z,S} = 0.6) = 131.7$ and $Re_{i,c}^{TVF}(s_{z,S} = 0.6) = 133.4$, cf. point α in Fig. 2(a)). Both, SPI and wTVF, are bi-stable coexisting at given parameters and visualizations are shown in Fig. 3. These two solutions will serve as initial states to study the consequences of a modulated field. To analyze the dynamics, we will utilize the mode amplitude $|u_{1,1}|$ as this is present in both solutions, wTVF and SPI. Worth to mention that for wTVF both mode amplitudes $|u_{1,1}|$ and $|u_{1,-1}|$ are identical (see Fig. 3(2a)).

3.2.1. Small modulation amplitude ($s_{z,M} = 0.1$) - fully supercritical

For small modulation amplitude ($s_{z,M} = 0.1$, $s_{z,S} = 0.6$) the system *remains always supercritical* for SPI although for (w)TVF it crosses the stability threshold for TVF within one period (cf. dashed arrows Fig. 2(a)).

3.2.1.1. 1-SPI. Fig. 4 shows the oscillation of the control function $s_z(t)$ together with the system response, illustrated by the mode amplitudes $|u_{1,1}|$ as a function of the reduced time t/T_H ($T_H = 2\pi/\Omega_H$ being the associated modulation period). The temporal oscillations are shown for different frequencies Ω_H as indicated. As the mode amplitude $|u_{1,1}|$ (cf. Fig. 3(a)) is present either in SPI (dashed curves) and wTVF (solid curves) it is used to characterize the dynamic behavior in Fig. 4.

Because for SPI the system always remains supercritical, the system response is very similar to the earlier studied case for supercritical TVF [49]. In the high-frequency limit, the stability behavior is solely affected by the time average of $s_z(t)$. Here the stability boundary coincides with a static stability boundary using an equivalent static magnetic Niklas parameter, which is larger than the mean value $\langle s_z(t) \rangle_{T_H} = 0.6$. For SPI the equivalent static driving is $s_{z,S} = 0.607$, which, for the sake of reference this is also included (red dashed lines in Fig. 4).

The larger parameter for equivalent static driving and the fact that the influence of alternating field decreases with increasing driving frequency leads back to the relaxation time (Néel and/or Brownian [55]) of the ferrofluid particles. In the high frequency case, the ferro colloid does not have enough time for remagnetization. This reduction

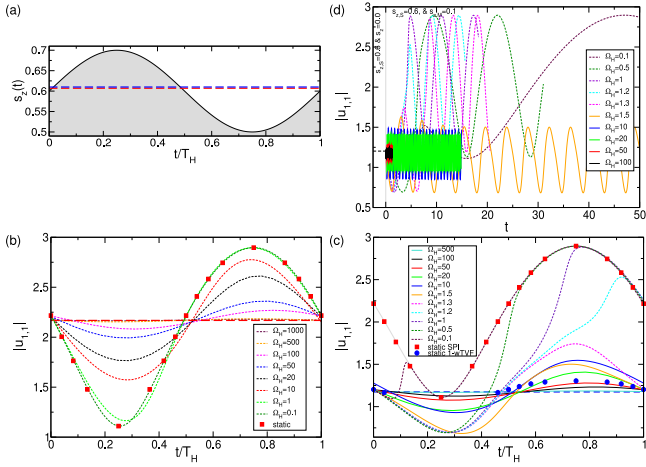


Fig. 4. Non-linear system response for supercritical solutions SPI and wTVF. (a) Temporal oscillations of the control function $s_z(t) = s_{z,S} + s_{z,M} \sin(\Omega_H t)$ ($s_{z,S} = 0.6, s_{z,M} = 0.1$, cf. trajectory III in Fig. 1(b)). The dominant mode amplitudes $|u_{1,1}|$ for (b) SPI and (c) (initial) wTVF as function of the reduced time t/T_H ($T_H = 2\pi/\Omega_H$ being the modulation period associated with the corresponding frequency). The red squares (■) (b, c) and blue circles (●) (c) show the stationary response to stationary magnetic field with field strength given by the actual value of $s_z(t)$. Thick, horizontal dashed lines in (a, b, c) show the order parameter for stationary driving with the mean Niklas parameter: for SPI $\langle s_z(t) \rangle = 0.607$, and for wTVF $\langle s_z(t) \rangle = 0.611$. (d) Time evolution of the dominant mode amplitude $|u_{1,1}|$ as for different Ω_H as indicated. Either of these modulation starts at $t = 0$, before only the static field $s_{z,S} = 0.4$ ($s_{z,M} = 0.0$) is present. For clarity/visibility mode amplitudes $|u_{0,1}|$ are only shown for short times t in case of high frequencies Ω_H . Note, solid (dashed) lines correspond to solutions of wTVF and SPI, respectively. In (c, d) dashed lines also indicate the transition from wTVF towards SPI. Control parameter $Re_c = 141$.

of magnetization is accompanied by reduction of rotational viscosity which means that the stabilization is slightly different to the static case (for SPI: $\langle s_z(t) \rangle_{T_H} = 0.6$ while $s_{z,S} = 0.607$).

For high frequency modulation $\Omega_H \gtrsim 100$, the flow dynamics is nearly averaged. Differences between mode amplitude $|u_{1,1}|$ and the mean value are very small. For $\Omega_H = 100$ the modulation amplitude $\Delta|u_{1,1}|$ is barely 3% of its time mean (Fig. 4(b)). Further a small phase shift between the minimum and maximum of the mode amplitudes $|u_{1,1}|$ versus the maximum and minimum of field parameter $s_z(t)$ can be observed: the amplitudes are temporally delayed against the field because of the inertia of the fluid resisting the fast changing accelerating Kelvin force leading to this time lag. The phase shift decreases consistently with decreasing driving frequency Ω_H (cf. $|u_{1,1}|$ in Fig. 4(b)). Meanwhile, the corresponding oscillation amplitudes are increasing with smaller Ω_H . The lower the modulation frequency Ω_H , the closer the oscillation profiles approach the curve of a static magnetic field (red squares).

3.2.1.2. wTVF. For wTVF the scenario is different as within one modulation period T_H the system crosses the boundary, separating stable and unstable wTVF at $s_{z,S} \approx 0.65$ (see Fig. 2(a)). The system response with respect to driving frequency Ω_H for $s_{z,M} = 0.1$ ($s_z(t) \in [0.5; 0.7]$) and initial condition wTVF (4(c, d)) can be summarized as follows:

- $1.45 \lesssim \Omega_H$: the system remains *supercritical* in wTVF.
- $\Omega_H \lesssim 1.45$: the system *changes* from the initial wTVF to SPI and hereafter remains *supercritical* in SPI.

As seen for SPI, in the high-frequency limit solely the time average of $s_z(t)$ affects the stability behavior. For $\Omega_H \gtrsim 500$, any variation over one period is eliminated. For wTVF the equivalent static magnetic Niklas parameter is $s_{z,S} = 0.611$ (dashed blue lines) and therefore also larger than the mean value $\langle s_z(t) \rangle_{T_H} = 0.6$. However, for low frequencies $\Omega_H \lesssim 1.45$ the initial wTVF state loses stability and transitions towards

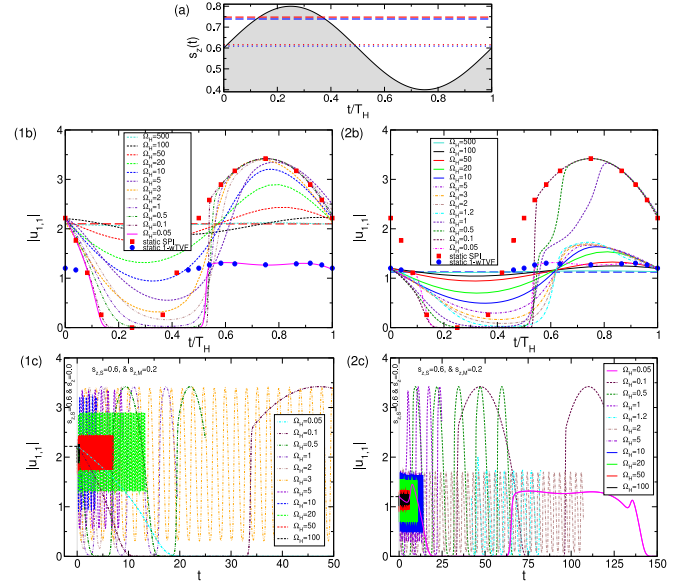


Fig. 5. Non-linear system response across the instability (cf. Fig. 4). (a) Temporal oscillations of the control function $s_z(t) = s_{z,S} + s_{z,M} \sin(\Omega_H t)$ ($s_{z,S} = 0.6, s_{z,M} = 0.2$, cf. trajectory IV in Fig. 1(b)). The dotted blue line marks the high frequency limit oscillatory ($s_{z,S} = 0.6, s_{z,M} = 0.2$) bifurcation threshold for SPI, while both dashed lines (red and blue) mark the stationary ($s_{z,S} = 0.6, s_{z,M} = 0.0$) bifurcation threshold for SPI and TVF, respectively. (b) Time evolution of the dominant mode amplitude $|u_{1,1}|$ as a function of time for different driving frequencies Ω_H as indicated. The modulation $s_{z,M}$ starts at $t = 0$, before only a static field $s_{z,S} = 0.6$ ($s_{z,M} = 0.0$) is present for (1) SPI and (2) wTVF, respectively. (c) Corresponding mode amplitudes $|u_{1,1}|$ as function of the reduced time t/T_H ($T_H = 2\pi/\Omega_H$ being the modulation period associated with the corresponding frequency). The red squares (■) and blue circles (●) in (b) show the stationary response to stationary magnetic field with magnetic field strength given by the actual value of $s_z(t)$. The horizontal dashed red (2a) and blue (2b) line indicate the (time averaged) mode amplitudes for high frequency driving. Control parameter $Re_c = 141$.

SPI while crossing the stability threshold for wTVF and thereafter the system response remains the same within the SPI as discussed before.

Interesting observation is the fact that for relative low frequencies $\Omega_H \lesssim 40$, the mode amplitudes $|u_{1,1}|$ within one period slightly *overshoot* the maximum values of their static counterparts. For smaller frequencies $40 \lesssim \Omega_H$ the mode amplitudes $|u_{1,1}|$ move around the average well within their maximum and minimum limits. This overshooting is caused by the inertia of the fluid itself.

For small modulation amplitude one can conclude, as the system remains supercritical *always* one single solution either SPI or wTVF is selected by the driving frequency Ω_H in agreement with earlier findings [38].

3.2.2. Large modulation amplitude ($s_{z,M} = 0.2$) - supercritical vs. subcritical

Consider system parameters around point α (Fig. 2(a)) and modulation amplitude $s_{z,M} = 0.2$ ($s_z(t) \in [0.4; 0.8]$), the non-linear system response becomes more complicated. Here the bifurcation thresholds for both, SPI ($s_{z,S} \approx 0.745$) and TVF ($s_{z,S} \approx 0.73$) are crossed within one modulation period (cf. Fig. 2(a)). As a result the system becomes temporal (slightly) subcritical. To be more precise, for an initial SPI *only* the bifurcation thresholds is crossed within the modulation while for wTVF additionally also the stability threshold ($s_{z,S} \approx 0.65$) (as for smaller modulation $s_{z,M} = 0.1$, cf. Fig. 4(c, d)) is crossed.

3.2.2.1. SPI. Depending on the driving frequency Ω_H , the system response for modulation amplitude $s_{z,M} = 0.2$ ($s_{z,S} = 0.6$) with SPI as *initial* solution, (Fig. 5(1)) can be summarized as follows:

- $2.5 \lesssim \Omega_H$: the system remains *supercritical* in SPI.

- $0.1 \lesssim \Omega_H \lesssim 1.45$: the system response changes between being supercritical (SPI) and subcritical (CCF).
- $0.06 \lesssim \Omega_H \lesssim 0.1$: the system features *intermittency* as the response changes between being supercritical and subcritical with random appearance of either SPI and wTVF (for further discussion see Section 3.2.3 below).
- $\Omega_H \lesssim 0.06$: the system response changes between being supercritical (wTVF) and subcritical (CCF).

Remaining supercritical, the initial system response is analog to the previous discussed scenario for SPI and smaller modulation amplitude $s_{z,M} = 0.1$ (Fig. 4). As seen before, in the high-frequency limit, it is only the time average of $s_z(t)$ that affects the stability behavior. For SPI the equivalent static driving is $s_{z,S} = 0.612$ (red dashed lines in Fig. 5). Note this is, as to expect larger than the corresponding value for smaller modulation amplitude $s_{z,M} = 0.1$.

Decreasing the driving frequency Ω_H the amplitude in the oscillating in $|u_{1,1}|$ continuously increase before at $\Omega_H \approx 2.5$ it eventually becomes temporally zero, representing that the system becomes subcritical (CCF). The smaller the driving frequency Ω_H , the longer the system remains subcritical (Fig. 5(b)). For low driving frequencies Ω_H , within one period, a fast growth of the mode amplitude $|u_{1,1}|$ is followed by a relaxing just similarly to values close to the stationary scenario (red squares), which becomes more and more approached with decreasing Ω_H . Similar to the scenario for full supercritical SPI (Fig. 5(b)), one can also observe a temporal delay of the mode amplitudes $|u_{1,1}|$ with respect to the extrema (min and max) of $s_z(t)$.

For lower driving frequencies the system features intermittency in a narrow region for Ω_H (see Section 3.2.3 below) before for very low frequencies the system response changes in favor of wTVF (Fig. 5(c)), which basically follows the values for stationary scenario, if being supercritical. Worth to emphasize that once changed to wTVF the system response remains the same for parameters $\Omega_H \lesssim 0.06$. Various simulations have been carried out with more than 50 cycles changing between subcritical and supercritical wTVF. Here no SPI has been detected.

3.2.2.2. wTVF. With variation in the driving frequency Ω_H , the system response for $s_{z,M} = 0.2$ ($s_z(t) \in [0.4; 0.8]$) and initial condition wTVF (5(2)) can be summarized as follows:

- $6.5 \lesssim \Omega_H$: the system remains *supercritical* in wTVF.
- for $1.1 \lesssim \Omega_H \lesssim 6.5$: the system response changes between being supercritical (wTVF) and subcritical (CCF).
- for $0.1 \lesssim \Omega_H \lesssim 1.1$: the system response changes between being supercritical (SPI) and subcritical (CCF).
- $0.06 \lesssim \Omega_H \lesssim 0.1$: (as for initial SPI and $s_{z,M} = 0.2$) the system shows intermittent behavior as the response changes between being supercritical and subcritical with random appearance of either SPI and wTVF (for further discussion see Section 3.2.3 below).
- $\Omega_H \lesssim 0.06$: (as for initial SPI and $s_{z,M} = 0.2$) the system response changes between being supercritical (wTVF) and subcritical (CCF).

As already seen for small modulation amplitude, the stability behavior for wTVF in the high-frequency limit is only affected by the time average of $s_z(t)$ and is equivalent to a static driving with $s_{z,S} = 0.614$ (blue dashed lines in Fig. 5), which is slightly smaller than the corresponding value one for SPI.

With decreasing driving frequency Ω_H the system response changes between subcritical CCF and supercritical wTVF for $1.1 \lesssim \Omega_H \lesssim 6.5$. Although the system response continuous to switch between supercritical and subcritical, for smaller values $0.1 \lesssim \Omega_H \lesssim 1.1$, the supercritical SPI appears, despite wTVF being the initial state.

Regardless the initial state, wTVF or SPI, for the narrow region $0.06 \lesssim \Omega_H \lesssim 0.1$ intermittent behavior is found with random exchange

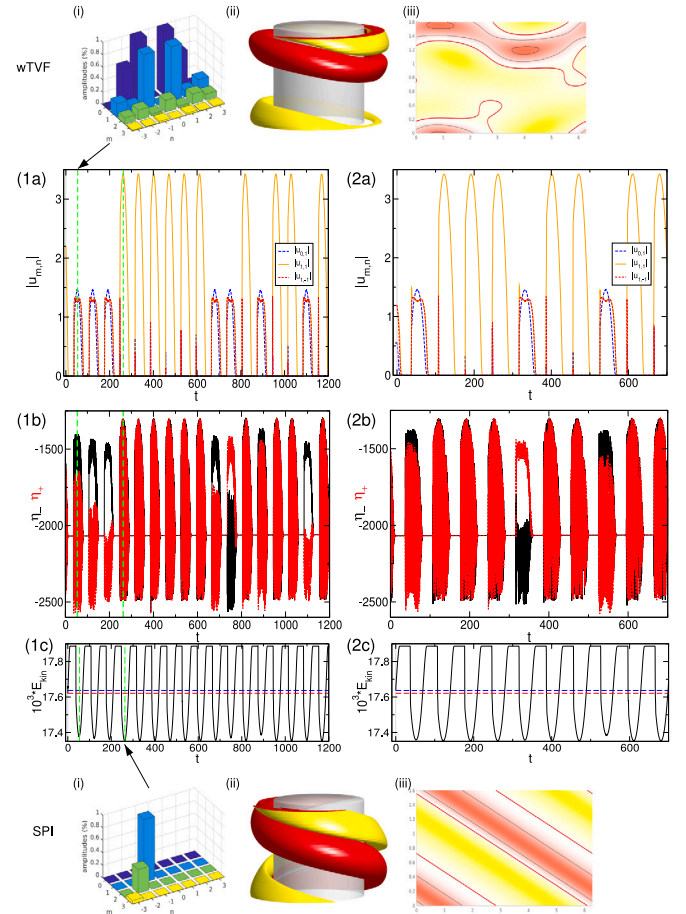


Fig. 6. Intermittent behavior with initial states (1) SPI and (2) wTVF. Time evolution of (a) characteristic mode amplitudes $|u_{m,n}|$, (b) azimuthal vorticity $\eta_{\pm} = \eta(0, 0, \pm 0.5)$ and (c) modal kinetic energy E_{kin} for modulating magnetic field with $s_{z,S} = 0.6$, $s_{z,M} = 0.2$ and modulation frequency $\Omega_H = 0.09$ (see also Fig. 7). Top and bottom correspond to two different solutions wTVF (top) and SPI, which appear during the time evolution as indicated in (1) (green dashed vertical lines).

of wTVF or SPI as the appearing supercritical solution. Further, for very low $\Omega_H \lesssim 0.06$ the system response is the same as seen before for SPI as initial condition. As before the system is alternating between subcritical CCF and supercritical wTVF.

3.2.3. Intermittency

Independent of the initial condition, SPI or wTVF, for a narrow region of driving frequency $0.06 \lesssim \Omega_H \lesssim 0.1$ the system is characterized by intermittency. While periodic alternating between subcritical CCF and supercritical solutions randomly either wTVF or SPI appear. Thereby both, the number of consecutive appearing same pattern (SPI or wTVF) and the number between switches from one to the other appear to be random. However, when ever the system becomes supercritical, both helical modes $|u_{1,\pm 1}|$ grow with identical magnitude together with the azimuthal (dominant) mode $|u_{0,1}|$ (Fig. 6(a)).

Fig. 6 shows an intermittency behavior as it appears for initial states (1) SPI and (2) wTVF, respectively. The time series of (a) $|u_{m,n}|$ and (b) η_{\pm} illustrates the random appearance of one of both states (SPI or wTVF) when the system is supercritical. Being supercritical, the modal kinetic energy $E_{kin} = \sum_m E_m = \frac{1}{2} \sum_m \int_0^{2\pi} \int_{-l/2}^{l/2} \int_{r_i}^{r_o} \mathbf{u}_m \mathbf{u}_m^* r dr dz d\theta$ [where \mathbf{u}_m (\mathbf{u}_m^*) is the m th (complex conjugate) Fourier mode of the velocity field] is basically the same for SPI and wTVF (c). Horizontal red and blue dashed lines indicate the modal kinetic energy of both initial states, SPI and wTVF, respectively, at $s_{z,t} = 0.6$. While for supercritical SPI, η_{\pm} are identical, they differ for wTVF. Thereby the difference depend on

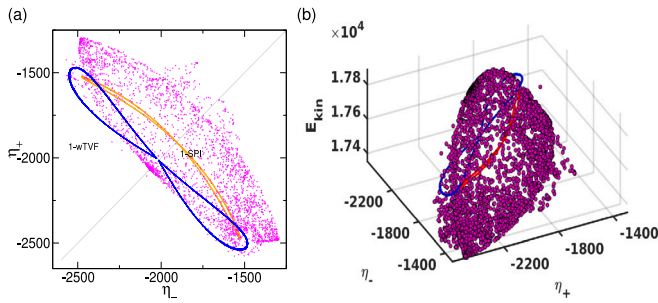


Fig. 7. (a) Phase portrait spanned by η_+ and η_- (see text for further description) and 3D parameter space (η_+ , η_- , E_{kin}). Curves for wTVF and SPI are obtained for stationary magnetic field $s_{z,S} = 0.6$ ($s_{z,M} = 0$), while magenta points represent the trajectory corresponding to modulating magnetic field with $s_{z,S} = 0.6$, $s_{z,M} = 0.2$ and modulation frequency $\Omega_H = 0.09$ at which intermittency is observed (see also Fig. 6).

the axial position of the azimuthal closed vortex structure, which can change due to the present axial periodic boundary condition.

The snapshots at top (wTVF) and bottom (SPI) (in Fig. 6) present supercritical states appearing within the time series at $s_z(t) = s_{z,max} = 0.4$ [$(s_{z,M} = -0.2)$ for minimum stabilization] as indicated (green dashed vertical lines). The similarity to the initial states (Fig. 3) is obvious. However, worth to mention that due to $s_z(t) = 0.4$ the solutions are more far away from their respectively onsets (Fig. 2(a)). As a result the absolute mode amplitudes $|u_{1,\pm}|$ for SPI and $|u_{0,\pm}|$ for wTVF are larger. In particular for the latter one can see that the dominant mode amplitudes are $u_{0,\pm 1}$ for $s_z(t) = 0.4$, while for $s_{z,S} = 0.6$ these are the mode amplitudes $|u_{1,\pm 1}|$.

In order to get some insight into the flow dynamics during the intermittent scenario, Fig. 7 shows the phase portrait spanned by η_+ and η_- (cf. Fig. 6(b)) and the 3D parameter space (η_+ , η_- , E_{kin}). The curves for wTVF and SPI belong to stationary magnetic field $s_{z,S} = 0.6$ ($s_{z,M} = 0$). Both solutions appear reflection symmetry with respect to the diagonal $\eta_+ = \eta_-$. The distance from the phase portraits to the diagonal line $\eta_- = \eta_+$ is a measure of the degree to which Z_2 symmetry is broken. The cloud of magenta points represent the trajectory corresponding to modulating magnetic field with $s_z(t) \in [0.4; 0.8]$ $s_{z,S} = 0.6$, $s_{z,M} = \pm 0.2$ and modulation frequency $\Omega_H = 0.09$ with intermittency (Fig. 6). While the system changes between subcritical and supercritical the basic symmetry remains preserved visible by the arrangement around the diagonal η_+ and η_- . In the 3D parameter space (η_+ , η_- , E_{kin}) the corresponding trajectory builds up to a ‘mountain’, which indicates the increasing phase space explored with becoming more supercritical, i.e. going from top to bottom of the mountain.

4. Discussion

Fig. 8 summarizes the detected non-linear system response for both initial conditions, SPI and wTVF, respectively, with small and large modulation amplitudes with respect to variation in the corresponding driving frequency Ω_H . For all in common the high frequency limit results in a *single* supercritical solution, which is determined by the corresponding initial condition, either SPI or wTVF.

For small modulation amplitude and $s_{z,M} = 0.1$ (Fig. 8(1)) the system always remains supercritical and the system response is relatively *simple*. In case of SPI (1a) as initial condition the system response is *independent* of Ω_H . Although remaining supercritical, this change for wTVF as initial condition (1b) as within one modulation period T_H the stability threshold for wTVF is crossed. As a result, for studied parameters, for $\Omega_H \lesssim 1.45$ the system response change to SPI.

For larger modulation amplitude and $s_{z,M} = 0.2$ the system response becomes significant more complicate as now within one modulation period T_H the system crosses also the bifurcation thresholds for both,

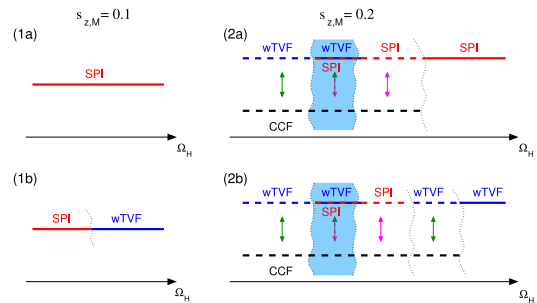


Fig. 8. Schematic illustration for stability change/switch between different flow states, subcritical and supercritical dynamical system response, with variation in the driving frequency Ω_H (increasing left to right) for small (1) $s_{z,M} = 0.1$ and large (2) $s_{z,M} = 0.2$ modulation amplitude (cf. Figs. 4 and 5). Initial states are (a) SPI and (b) wTVF, respectively. Solid lines indicate a single stable solution and dashed lines indicate an alternation between different solutions.

SPI and TVF, and as a result changes between temporally supercritical and subcritical behavior. In the high frequency limit SPI (2a) (as initial condition) remains unaffected. With decreasing Ω_H the initial system response is an alternation between subcritical CCF and supercritical SPI (due to crossing the bifurcation threshold). Further, reducing Ω_H the system shows intermittent behavior (in a narrow parameter range) with random appearance of both supercritical SPI and wTVF, which is eventually followed by alternation between CCF and supercritical wTVF.

Similar to SPI, also wTVF (2b) remains preserved in the high frequency limit. With reducing Ω_H the system response with alternation between sub- and supercritical solutions. Initially between CCF and wTVF, which then change towards CCF and SPI. This sequence results from the fact that the corresponding bifurcation threshold for SPI lies below the one for TVF (Fig. 2(a)). Thus, for smaller frequencies Ω_H , i.e. larger period times T_H the helical modes $|u_{1,\pm 1}|$ have enough time to grow before the azimuthal modes $|u_{0,\pm 1}|$ can do so. Hereafter the non-linear system response is identical as described before. A narrow region of intermittency is followed by the final alternation between CCF and supercritical wTVF at very low driving frequency Ω_H .

Most interesting observations are the appearing of intermittent behavior for a narrow parameter range in driving frequency Ω_H as well that for low driving frequency Ω_H (and large modulation amplitude and $s_{z,M} = 0.2$) the system *always* evolves into wTVF as supercritical solution, *independent* of the initial state (SPI or wTVF). This is even more strange for the following reasons: First, as a matter of fact the stability threshold for SPI is lower than the corresponding one of TVF (cf. Fig. 2(a)). Second, the SPI branch bifurcates stable, while the TVF branch bifurcates unstable (as appearing second). As a result one might expect the stable SPI to be favored. In fact, we detected both modes $|u_{1,\pm 1}|$ initially to grow. But eventually, before one of both modes $|u_{1,+1}|$ or $|u_{1,-1}|$ overcomes the other in order to select a left or right-winding SPI, the modes $u_{0,\pm 1}$ grow to generate wTVF (with $|u_{1,+1}| = |u_{1,-1}|$). Such a competition is also found in the intermittent regime (cf. Fig. 7(1a, 2a)), although there sometimes one of the helical modes $|u_{1,\pm 1}|$ leaves as the ‘winner’ generating SPI.

A possible explanation for the intermittent behavior may be the following. For given parameters, the system crosses first the bifurcation and at the same time also stability threshold for SPI and second the bifurcation threshold for TVF (Fig. 2(a)). Thus, the helical modes $|u_{1,\pm 1}|$ should grow (first), as they do and in fact they grow with identical amplitudes. Having (later) crossed the bifurcation threshold for TVF, also the azimuthal modes $|u_{0,\pm 1}|$ grow. Any appearing small perturbations introduced by these now raising modes may affect the helical modes $|u_{1,\pm 1}|$ to become *unequal*. Once unequal (even with minor differences), the larger one continuously grows to become the major mode, while the smaller one dies out together with the modes $|u_{0,\pm 1}|$. The result is a SPI.

On the other hand if no larger (random) perturbations appear during the growth, the mode amplitudes $u_{1,1}$ and $u_{1,-1}$ remain equal while $|u_{0,\pm 1}|$ grow. In this case wTVF appears. This speculation is supported by the fact that for small driving frequencies $\Omega_H \lesssim 0.06$ the system response is found to be always wTVF when becoming supercritical. Thus, for such low frequencies, corresponding long period times T_H the additional introduced perturbations with changing $s_z(t)$ have enough time to die out and therefore the helical modes $|u_{1,1}|$ and $|u_{1,-1}|$ can grow with identical amplitudes. Together with the growing $|u_{0,\pm 1}|$ this result in the found wTVF.

The present work manifests the importance of complex fluids under external driving. The effect of modulated external fields on the evolution of disturbances and nonlinear dynamics is of great interest in connection with the possibility of controlling the hydrodynamic processes and mass transfer. As such the modulation in frequency for an alternating field may provide a simple and accurate way to trigger the system response. As shown in the present work the flow can be controlled (i) between different supercritical flow solutions or (ii) between supercritical and subcritical flow solutions, which means to trigger either sub- or supercritical system response. Aside the different flow pattern of these flow structures they typically also have crucial different fluid properties. With respect to industrial and engineering application most prominent to mention is their significant distinguishable torque. This, together with the ability to modify their characteristics (in a simple and very accurate/controllable way) due to an oscillating magnetic field makes ferrofluids highly interesting in the area of flow control and/or damping systems, e.g. in aerospace sector, with very strict requirement on weight, size and reliability.

Since ferrofluid has the unique property of being controlled by an external applied oscillating magnetic field, future studies will focus on the correlation of this frequency with the internal heat transfer within the ferrofluid. Here, the key focus is the use of ferrofluids in medical applications, e.g. in cancer treatment by hyperthermia. Having brought ferrofluid particles in the tumor tissue they can be used to heat up the tissue via alternating in the frequency and thus destroy the tumor, avoiding side effects to other organs. Aside, from a more fundamental point of view is the study of time-dependent flow states, e.g. wavy Taylor vortices and their response to stimulation with its own or higher harmonic frequencies. For this scenario interesting resonant phenomena and/or switching between different modes can be highly expected.

CRedit authorship contribution statement

Sebastian Altmeyer: Is the alone responsible for the whole paper, Conceptualization, Methodology, Software, Data creation, Writing – original draft, Visualization, Investigation, Software, Validation, Writing – review & editing.

Declaration of competing interest

The authors declare that they have no known competing financial interests or personal relationships that could have appeared to influence the work reported in this paper.

Acknowledgments

S. A. is a Serra Hünter Fellow.

Appendix

Comparison with experimental observations

The appendix provides a short discussion and comparison of the here considered parameters in its dimensionless forms with dimensional experimental values. Aside a comparison with experimental observation is given to validate the code.

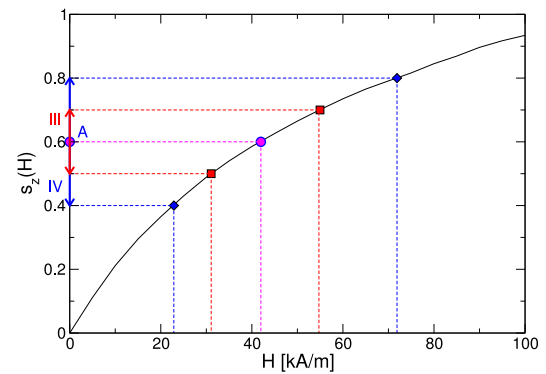


Fig. 9. The Niklas function s_z versus the magnetic field strength H for ferrofluid APG933 [34]. Point A gives the parameters for supercritical flows at $Re_i = 141$ while III and IV correspond to the set of parameters explored in detail (see also Fig. 1). In detail the values are in A: $s_z = 0.6 \Leftrightarrow H = 41.98$; for III: $s_{z,min} = 0.5 \Leftrightarrow H = 31.07$ & $s_{z,max} = 0.7 \Leftrightarrow H = 54.97$; for IV: $s_{z,min} = 0.4 \Leftrightarrow H = 22.88$ & $s_{z,max} = 0.8 \Leftrightarrow H = 71.98$.

A.1. Relation between niklas function $s_z(H)$ and experimental field strength H

Doubtless most important is the relation of the Niklas function $s_z(H)$ and the corresponding experimental magnetic field strength H . The range of the magnetic parameter s_z considered in this paper, i.e., $0 \leq s_z \leq 1.0$, can in fact be realized in experimental studies of ferrofluids. Fig. 9 shows, for ferrofluid APG933 [34], the relation between $s_z(H)$ and H . For example, our computationally determined value of oscillating fields (at $Re_i = 141$) range for (III) from $s_{z,min} = 0.5$ to $s_{z,max} = 0.7$, which corresponds to the magnetic field strength of about $H = 31.07$ [kA/m] and $H = 54.97$ [kA/m], respectively. Consequently the range for (IV) is wider from $s_{z,min} = 0.4$ to $s_{z,max} = 0.8$, which corresponds to the magnetic field strength of about $H = 22.88$ [kA/m] and $H = 71.98$ [kA/m], respectively. Worth mentioning, that the relation demonstrated in Fig. 9 depends on the ferrofluid type. For different ferrofluids, for example Cobalt based ferrofluids [21], the effects due to magnetic fields can be “stronger”, meaning that similar dynamical behaviors can occur but for weaker magnetic fields. Aside the axial wavenumber, here $k = 3.927$ corresponding to an axial wavelength $\lambda = 1.6 = 2\pi/k$ may also influence the nonlinear response of the system. For sure it effects the stability thresholds and it is to expect that larger vortex cells, i.e. larger [smaller] λ [k] will be more inert to the external driving frequency of the alternating field. The latter point is beyond the scope of the present work but in focus on future investigations.

A.2. Code validation

For code validation some of the experimental results presented by Reindl & Odenbach [20] have been reproduced. In their work they studied ferrofluidic Couette flow with large aspect ratio $\Gamma = 20$ under the influence of an axial magnetic field. In absence of any field they detected a critical rotation rate (here the primary bifurcating flow, Taylor-vortex flow (TVF) appears) of $\omega_{i,c} = 0.498 \pm 0.004$ Hz with axial wavenumber $k = 3.14$ (i.e. 10 vortex pairs present in the gap) and outer cylinder at rest, $\omega_o = 0$, which is equivalent to a critical Reynolds number $Re_{i,c}^{exp} = 68.4$ (ferrofluid parameters as indicated in table 2 [20]). Consider their studied system parameter our code provides a critical Reynolds number $Re_{i,c}^{num,RBC} = 68.6$ whereby we detect a wavenumber $k = 3.15$ in the system (in the center, ignoring the Ekman vortices near the lids which have slightly different k) for rigid boundary conditions. This is a variation fairly less than 0.5%. In addition, assuming periodic boundary conditions we obtained $Re_{i,c}^{num,PBC} = 68.5$. Fig. 10 illustrates the critical Reynolds number, $Re_{i,c}$, at which Taylor vortex flow (TVF)

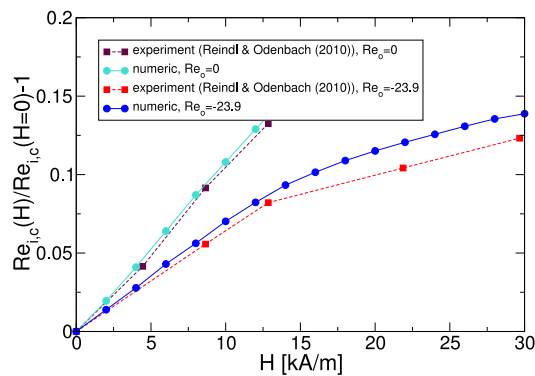


Fig. 10. Variation with axial magnetic field strength H of the reduced critical Reynolds number for $k = 3.15$ (numerics) and $k = 3.14$ (experiment) and outer Reynolds number $Re_o = 0$ and -23.9 , respectively. RBC and $\Gamma = 20$; used ferrofluid parameters as indicated in table 2 [20].

sets in, in a reduced form $(Re_{i,c}(H)/Re_{i,c}(H = 0) - 1)$ as a function of applied magnetic field strength for two parameter settings $Re_o = 0$ (outer cylinder at rest) and $Re_o = -23.9$ (counter-rotating cylinders). Here the numerical code provides an onset of $Re_{i,c} = 69.3$. As Fig. 10 illustrates, experimental and numerical results are in good agreement. However, a general observation is that the stabilizing effect is slightly stronger based on the numerical results compared to experimental values, i.e. the numerical curves lie above the experimental ones. But they are well within the error-range given for experimental data provided in [20].

References

- [1] G.I. Taylor, Stability of a viscous liquid contained between two rotating cylinders, *Philos. Trans. R. Soc. Lond. A* 223 (1923) 289.
- [2] P. Chossat, G. Iooss, *The Couette–Taylor Problem*, Springer, Berlin, 1994.
- [3] H.C. Hu, R.E. Kelly, Effect of a time-periodic axial shear flow upon the onset of Taylor vortices, *Phys. Rev. E* 51 (1995) 3242.
- [4] F. Marques, J. Lopez, Spatial and temporal resonances in a periodically forced hydrodynamic system, 136 (2000) 340.
- [5] A.Y. K. I. Weisberg, A. Smits, Delaying transition in Taylor–Couette flow with axial motion of the inner cylinder, *J. Fluid Mech.* 348 (1997) 141.
- [6] B.T. Murray, G.B. McFadden, S.R. Coriell, Stabilization of Taylor–Couette flow due to time-periodic outer cylinder oscillation, *Phys. Fluids A* 2 (1990) 2147.
- [7] R. Donnelly, Experiments on the stability of viscous flow between rotating cylinders. III, Enhancement of stability by modulation, *Proc. R. Soc. Lond. Ser. A Math. Phys. Eng. Sci.* 281 (1964) 130.
- [8] R.J. R. F. Donnelly, H. Suhl, Enhancement of hydrodynamic stability by modulations, *Phys. Rev. Lett.* 9 (1962) 363–365.
- [9] A. G. T. Ganske, S. Grossmann, Modulation effects along stability border in Taylor–Couette flow, *Phys. Fluids* 6 (1994) 3823.
- [10] S. Carmi, J.I. Tustaniwskyj, Stability of modulated finite-gap cylindrical Couette flow: linear theory, *J. Fluid Mech.* 108 (1981) 19.
- [11] C.F. Barenghi, C.A. Jones, Modulated Taylor–Couette flow, *J. Fluid Mech.* 208 (1989) 127.
- [12] C.F. Barenghi, Computations of transitions and Taylor vortices in temporally modulated Taylor–Couette flow, *J. Comput. Phys.* 95 (1991) 175.
- [13] R.E. Rosensweig, *Ferrohydrodynamics*, Cambridge University Press, Cambridge, 1985.
- [14] S. Altmeyer, *Ferrofluids*, Scholarpedia 15 (2020) 55163.
- [15] J.L. Neuringer, R.E. Rosensweig, *Ferrohydrodynamics*, *Phys. Fluids* 7 (1964) 1927.
- [16] R.E. Rosensweig, R. Kaiser, G. Miskolczy, Magnetoviscosity of magnetic fluid in a magnetic field, *J. Colloid Interface Sci.* 29 (1969) 680.
- [17] M. Niklas, Influence of magnetic fields on Taylor vortex formation in magnetic fluids, *Z. Phys. B* 68 (1987) 493.
- [18] S. Odenbach, Magnetoviscous and viscoelastic effects in ferrofluids, *Internat. J. Modern Phys. B* 14 (2000) 1615.
- [19] S. Odenbach, H. Gilly, Taylor–vortex flow of magnetic fluids under the influence of an azimuthal magnetic field, *J. Magn. Magn. Mater.* 152 (1995) 123.
- [20] M. Reindl, S. Odenbach, Influence of a homogeneous axial magnetic field on Taylor–Couette flow of ferrofluids with low particle–particle interaction, *Exp. Fluids* 50 (2011) 375.
- [21] M. Reindl, S. Odenbach, Effect of axial and transverse magnetic fields on the flow behavior of ferrofluids featuring different levels of interparticle interaction, *Phys. Fluids* 23 (2011) 093102.
- [22] S. Altmeyer, C. Hoffmann, A. Leschhorn, M. Lücke, Influence of homogeneous magnetic fields on the flow of a ferrofluid in the Taylor–Couette system, *Phys. Rev. E* 82 (2010) 016321.
- [23] S. Altmeyer, J. Lopez, Y. Do, Influence of an inhomogeneous internal magnetic field on the flow dynamics of ferrofluid between differentially rotating cylinders, *Phys. Rev. E* 85 (2012) 066314.
- [24] S. Altmeyer, A. Leschhorn, C. Hoffmann, M. Lücke, Elongational flow effects on the vortex growth out of Couette flow in ferrofluids, *Phys. Rev. E* 87 (2013) 053010.
- [25] S. Altmeyer, J. Lopez, Y. Do, Effect of elongational flow on ferrofluids under a magnetic field, *Phys. Rev. E* 88 (2013) 013003.
- [26] S. Altmeyer, Agglomeration effects in rotating ferrofluids, *J. Magn. Magn. Mater.* 482 (2019) 239.
- [27] M.I. Shliomis, Effective viscosity of magnetic suspensions, *Sov. Phys.—JETP* 34 (1972) 1291.
- [28] M.I. Shliomis, Comment on magnetoviscosity and relaxation in ferrofluids, *Phys. Rev. E* 64 (2001) 063501.
- [29] M.I. Shliomis, K.I. Morozov, Negative viscosity of ferrofluid under alternating magnetic field, *Phys. Fluids* 6 (1994) 2855.
- [30] M. Kole, S. Khandekar, Engineering applications of ferrofluids: A review, *J. Magn. Magn. Mater.* 537 (2021) 168222.
- [31] E.K. Ruuge, A.N. Rusetski, Magnetic fluids as drug carriers: Targeted transport of drugs by a magnetic field, *J. Magn. Magn. Mater.* 122 (1993) 335.
- [32] D.C.F. Chan, D.B. Kirpotin, P.A. Bunn, Synthesis and evaluation of colloidal magnetic iron oxides for the site-specific radiofrequency-induced hyperthermia of cancer, *J. Magn. Magn. Mater.* 122 (1993) 374.
- [33] M. Wu, E. Huynh, S. Tang V. Uskoković, Brain and bone cancer targeting by a ferrofluid composed of superparamagnetic iron-oxide/silica/carbon nanoparticles (earthelics), *Acta Biomater.* 88 (2019) 422–447.
- [34] The specifications for the ferrofluid APG933 are as follows: $\mu_0 M_s = 20\text{mT}$, $\eta = 500\text{mPas}$, density $\rho = 1.09\text{g/cm}^3$, $\Phi_m = 3.3\%$, susceptibility $\chi = 0.9$, mean diameter of the particle’s magnetic core 10 nm, thickness of the polymeric coating 2 nm.
- [35] L. Zhang, T. Nazar, N.M. Bhatti, E.E. Michaelides, Stability analysis on the kerosene nanofluid flow with hybrid zinc/aluminum-oxide (ZnO-al₂O₃) nanoparticles under Lorentz force, *Internat. J. Numer. Methods Heat Fluid Flow* 32 (2) (2022) 740–760.
- [36] R. Rosensweig, Heating magnetic fluid with alternating magnetic field, *J. Magn. Magn. Mater.* 252 (2002) 370, Proceedings of the 9th International Conference on Magnetic Fluids.
- [37] M. Goharkhah, A. Salarian, M. Ashjaee, M. Shahabadi, Convective heat transfer characteristics of magnetite nanofluid under the influence of constant and alternating magnetic field, *Powder Technol.* 274 (2015) 258.
- [38] S. Altmeyer, On the ridge of instability in ferrofluidic couette flow via alternating magnetic field, *Sci. Rep.* 11 (2021) 4705.
- [39] D. Ghosh, P.K. Das, Control of flow and suppression of separation for couette–poiseuille hydrodynamics of ferrofluids using tunable magnetic fields, *Phys. Fluids* 31 (2019) 083609.
- [40] C. Huang, J. Yao, T. Zhang, Y. Chen, H. Jiang, D. Li, Damping applications of ferrofluids: A review, *J. Magn.* 22 (1) (2017) 109–121.
- [41] C.D. Andereck, S.S. Liu, H.L. Swinney, Flow regimes in a circular couette system with independently rotating cylinders, *J. Fluid Mech.* 164 (1986) 155.
- [42] C. Hoffmann, S. Altmeyer, A. Pinter, M. Lücke, Transitions between Taylor vortices and spirals via wavy Taylor vortices and wavy spirals, *New J. Phys.* 11 (2009) 053002.
- [43] H.W. Müller, M. Liu, Structure of ferrofluid dynamics, *Phys. Rev. E* 64 (2001) 061405.
- [44] P. Langevin, Magnétisme et théorie des électrons, *Ann. Chem. Phys.* 5 (1905) 70.
- [45] J. Embs, H.W. Müller, C. Wagner, K. Knorr, M. Lücke, Measuring the rotational viscosity of ferrofluids without shear flow, *Phys. Rev. E* 61 (2000) R2196.
- [46] M. Niklas, H. Müller-Krumbhaar, M. Lücke, Taylor–vortex flow of ferrofluids in the presence of general magnetic fields, *J. Magn. Magn. Mater.* 81 (1989) 29.
- [47] S. Odenbach, H.W. Müller, Stationary off-equilibrium magnetization in ferrofluids under rotational and elongational flow, *Phys. Rev. Lett.* 89 (2002) 037202.
- [48] S. Altmeyer, A. Leschhorn, C. Hoffmann, M. Lücke, Elongational flow effects on the vortex growth out of Couette flow in ferrofluids, *Phys. Rev. E* 87 (2013) 053010.
- [49] S. Altmeyer, Increasing flow complexity in time-dependent modulated ferrofluidic couette flow, *Fluid Dyn.* (2022) accepted.
- [50] J.W. Swift, K. Wisenfeld, Suppression of period doubling in symmetric systems, *Phys. Rev. Lett.* 52 (1984) 705.
- [51] M. Golubitsky, I. Stewart, D. Schaeffer, *Singularities and Groups in Bifurcation Theory II*, Springer, New York, 1988.
- [52] R. Tagg, The couette–Taylor problem, *Nonlinear Sci. Today* 4 (1994) 1.
- [53] S. Altmeyer, C. Hoffmann, On secondary instabilities generating footbridges between spiral vortex flow, *Fluid Dyn. Res.* 46 (2014) 025503.
- [54] Y. Demay, G. Iooss, Calcul des solutions bifurquées pour le problème de couette–Taylor avec les deux cylindres en rotation, *J. Méc. Théor. Appl.* (1984) 193–216.
- [55] M.I. Shliomis, Magnetic fluids, *Sov. Phys. Usp.* 112 (1974) 153.